SAFE STRUCTURAL DESIGN FOR FATIGUE AND CREEP USING CYCLIC YIELD STRENGTH

Yevgen Gorash **and Donald MacKenzie***

Department of Mechanical and Aerospace Engineering, University of Strathclyde, Glasgow, Scotland, UK

ABSTRACT

This study proposes cyclic yield strength (CYS, $\sigma_{\mathrm{y}}^{\mathrm{c}}$) as a potential characteristic of safe design for structures operating under fatigue and creep conditions. CYS is defined on a cyclic stress-strain curve (SSC), while monotonic yield strength (MYS, $\sigma_{\mathrm{y}}^{\mathrm{m}}$) is defined on a monotonic SSC. Both values of $\sigma_{\mathrm{y}}^{\mathrm{c}}$ and $\sigma_{\mathrm{y}}^{\mathrm{m}}$ are identified using a 2-step fitting procedure of the experimental SSCs using Ramberg-Osgood and Chaboche material models. A typical S-N curve in stress-life approach for fatigue analysis has a distinctive minimum stress lower bound, the fatigue endurance limit (FEL, $\sigma_{\mathrm{lim}}^{\mathrm{f}}$). Comparison of $\sigma_{\mathrm{y}}^{\mathrm{c}}$ and $\sigma_{\mathrm{lim}}^{\mathrm{f}}$ reveals that they are approximately equal. Thus, safe fatigue design is guaranteed in the purely elastic domain defined by the $\sigma_{\mathrm{y}}^{\mathrm{c}}$. A typical long-term strength (LTS) curve in time-to-failure approach for creep analysis has 2 inflections corresponding to the $\sigma_{\mathrm{y}}^{\mathrm{c}}$ and $\sigma_{\mathrm{y}}^{\mathrm{m}}$. These inflections separate 3 sections on a LTS curve, which are characterised by different creep fracture modes and creep deformation mechanisms. Thus, safe creep design is guaranteed in the linear creep domain with brittle failure mode defined by the $\sigma_{\mathrm{y}}^{\mathrm{c}}$. These assumptions are confirmed using 3 structural steels for normal and high-temperature applications. The advantage of using $\sigma_{\mathrm{y}}^{\mathrm{c}}$ for characterisation of fatigue and creep strength is a relatively quick experimental identification. The total duration of cyclic tests for a cyclic SSC identification is much less than the typical durations of fatigue and creep rupture tests at the stress levels around the $\sigma_{\mathrm{y}}^{\mathrm{c}}$.
Keywords: Creep, Fatigue, Failure, Plasticity, Softening, Steel, Yield Strength.

INTRODUCTION

Characterisation of long-term strength of structural materials is an important engineering task for prevention of potential catastrophic failures of critical equipment. However, studies of this type are usually very long-lasting, technically challenging and involve expensive experimental work. Thus, the main scope of this study is the formulation of a simple way to predict characteristics of the long-term material behaviour (creep and fatigue, in the first instance) using basic material properties.

Based upon the extensive availability of experimental material data, a significant progress toward this challenge has been achieved so far and may be observed in the literature. Comparative study by Kim *et al.* [1] evaluated seven basic methods for estimating uniaxial fatigue properties (including $\sigma_{\mathrm{lim}}^{\mathrm{f}}$) from tensile properties or hardness. This study was based upon the fatigue test data for eight ductile steels under axial and torsional loading. Three of the evaluated methods were able to predict over 93% of test cases within a factor of 3 compared with observed lives. The formulas for $\sigma_{\mathrm{lim}}^{\mathrm{f}}$ prediction included mechanical properties such as elasticity modulus E, ultimate tensile strength σ_{u} and true fracture ductility ε_{f}. Among the variety of empirical formulations for $\sigma_{\mathrm{lim}}^{\mathrm{f}}$ prediction with different combinations of aforementioned mechanical properties, the simplest are based on σ_{u}: $\sigma_{\mathrm{lim}}^{\mathrm{f}} = 1.9018\,\sigma_{\mathrm{u}}$ (Universal slopes method); $\sigma_{\mathrm{lim}}^{\mathrm{f}} = 1.5\,\sigma_{\mathrm{u}}$ (Uniform material law); and $\sigma_{\mathrm{lim}}^{\mathrm{f}} = \sigma_{\mathrm{u}} + 345$ MPa (Mitchell's method), which shown an accuracy of $R^2 = 0.88$. Another simple method in this comparison, proposed by Roessle & Fatemi [2], used a Brinnell hardness

*Corresponding author. Tel.: +44 141 5484851. E-mail: yevgen.gorash@strath.ac.uk

HB for prediction as $\sigma^{\mathrm{f}}_{\mathrm{lim}} = 4.25\,HB + 225$ MPa. This approach showed a reasonable accuracy of $R^2 = 0.86$ for experimental data fit.

The study by Casagrande *et al.* [3] investigated a relationship between $\sigma^{\mathrm{f}}_{\mathrm{lim}}$ and Vickers hardness HV in steels and developed a method to predict $\sigma^{\mathrm{f}}_{\mathrm{lim}}$. A good correlation was observed between HV and $\sigma^{\mathrm{f}}_{\mathrm{lim}}$ for for four kinds of steels in different metallurgical states. However, the proposed empirical method is not straightforward and involves a number of parameters and equations to achieve a reasonable of accuracy of $\sigma^{\mathrm{f}}_{\mathrm{lim}}$ predictions. Recently, Bandara *et al.* [4] proposed a formula for predicting $\sigma^{\mathrm{f}}_{\mathrm{lim}}$ of steels in the gigacycle regime. It uses a combination of σ_{u} and HV as material parameters and was verified using the experimental results for 45 steels.

A different approach was developed by Li *et al.* [5], who estimated theoretically $\sigma^{\mathrm{c}}_{\mathrm{y}}$ and $\sigma^{\mathrm{f}}_{\mathrm{lim}}$ using test data for 27 alloy steels. One formula expresses $\sigma^{\mathrm{c}}_{\mathrm{y}}$ by two conventional mechanical performance parameters – σ_{u} and the reduction in area ψ. The other formula expresses the FEL by the CYS with a reasonable accuracy of $R^2 = 0.883$ as $\sigma^{\mathrm{f}}_{\mathrm{lim}} = 1.13\,(\sigma^{\mathrm{c}}_{\mathrm{y}})^{0.9}$. Despite the relative simplicity, the proposed relation can't be considered as mathematically elegant, most probably because of the conventional assumption of 0.2% plastic strain offset for $\sigma^{\mathrm{c}}_{\mathrm{y}}$ and $\sigma^{\mathrm{m}}_{\mathrm{y}}$. Nevertheless, this formula by Li *et al.* [5] demonstrated the tendency that $\sigma^{\mathrm{f}}_{\mathrm{lim}}$ is not too much different from $\sigma^{\mathrm{c}}_{\mathrm{y}}$.

Less progress has been achieved in methods for creep rupture strength evaluation, but recently an important observation was discovered by Kimura [6]. The creep strength of ferritic and austenitic steels has been investigated in [6] through the correlation between creep rupture curve, presenting stress vs. creep rupture life, and 50% of 0.2% offset yield stress (half yield) at a wide range of temperatures. The inflection of the creep rupture curve at half yield was recognised for ferritic creep resistant steels with martensitic or bainitic microstructure, e.g. T91, T92 and T122. This was explained in terms of different mechanisms of microstructural evolution during creep at high- and low-stress regimes. The purpose of this study was to point out a significant risk of overestimation of long-term creep rupture strength by extrapolating the data for martensitic and bainitic steels (e.g. ASTM T91/P91) in high-stress regime to low-stress regime, which are separated by half yield.

A similar problem with particular application to ASTM P91 steel was investigated and discussed by Gorash *et al.* [7, 8] for the purpose of a creep constitutive model development. In these works, apart from inflection of creep rupture curve, the simultaneous inflection of the minimum creep rate curve, presenting minimum creep rate vs. stress, was recognised. Alternation of minimum creep rate slope was explained in terms of different creep deformation mechanism (linear creep for low stress and power-law for high stress), while alternation of creep rupture life slope was explained in terms of different damage accumulation modes (brittle fracture for low stress and ductile for high stress). The inflection of both curves was characterised by the same value σ_0 called transition stress, which had the meaning of material parameter in the developed "double-power-law" creep model. However, σ_0 was identified in [7, 8] using minimum creep rate data, and no relation of σ_0 to basic mechanical properties of ASTM P91 steel was recognised.

The principal aim of the present study is to investigate a link in characterisation of long-term strength of structural steel by finding a similar quantative feature in available experimental data. This establishes a straight relation between characteristics of creep and fatigue behaviour on one hand and yield strength as a basic material property and characteristic of plasticity on other hand.

CONCEPT OF THE SAFE STRUCTURAL DESIGN

Definition of the yield strength

Dowling [9] discusses several methods to characterise the yield strength σ_{y}. The first is the *proportional limit* $\sigma^{\mathrm{p}}_{\mathrm{y}}$, which is the stress where the first departure from linearity occurs. The second is the *elastic limit* $\sigma^{\mathrm{el}}_{\mathrm{y}}$, which is the highest stress that does not cause plastic deformation. The third is the *offset yield strength* $\sigma^{0.2\%}_{\mathrm{y}}$, which is the stress in the point on stress-strain curve typically defined by the plastic strain offset of 0.2% from elastic line. This value is generally the most practical means

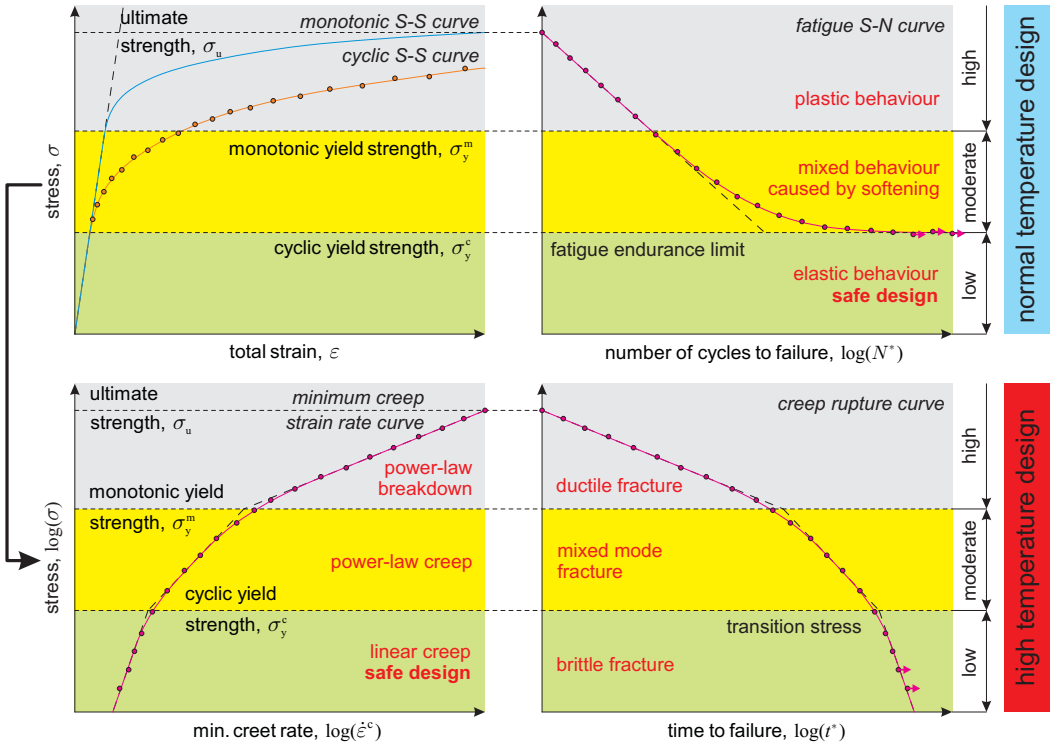

Figure 1: Concept of the safe structural design for fatigue and creep using cyclic yield strength

of defining the yielding event for engineering metals. Therefore, $\sigma_y^{0.2\%}$ is usually meant to define the yield strength σ_y in the literature. However, here the *elastic limit* σ_y^{el}, defined in the scope of unified Chaboche model [10, 11], is used as the yield strength σ_y.

This study proposes σ_y^c as a key characteristic for the definition of safe design for engineering structures operating under fatigue and creep conditions, as illustrated in Fig. 1. It is conventionally defined in context of a cyclic stress-strain curve (SSC), which is obtained from results of cyclic tests for a number of different strain ranges. Each cyclic test produces a stabilised stress response, which is effected either by hardening or by softening depending on the type of steel. In the case of steels with a cyclic softening effect, σ_y^c separates the low stress range of purely elastic behaviour from moderate stress range of mixed elasto-plastic behaviour. Monotonic yield strength σ_y^m, which is conventionally defined in context of a monotonic SSC, separates the moderate stress range of mixed elasto-plastic behaviour from the high stress range of purely plastic behaviour. Both values of σ_y^m and σ_y^c are identified using a 2-steps fitting procedure of the experimental S-S curves. The first step applies the Ramberg-Osgood material model, which produces basic smoothing and extrapolation, to the both monotonic and cyclic SSCs separately. The second step of fitting involves a typical rate-independent form of the Chaboche material model with 3 kinematic backstresses. Fitting the Chaboche model with two separate sets of material constants sequentially to the both SSCs provides the values of σ_y^m and σ_y^c with minimum offset from the elastic line as elastic limits.

Stress-strain curves fitting procedure

As experimental SSCs usually demonstrate some level of scatter, the first step in data fitting for the material parameters identification is basic curve smoothing. The conventional Ramberg-Osgood (R-O) equation [15] is optimal for such curve smoothing since it was formulated to describe the

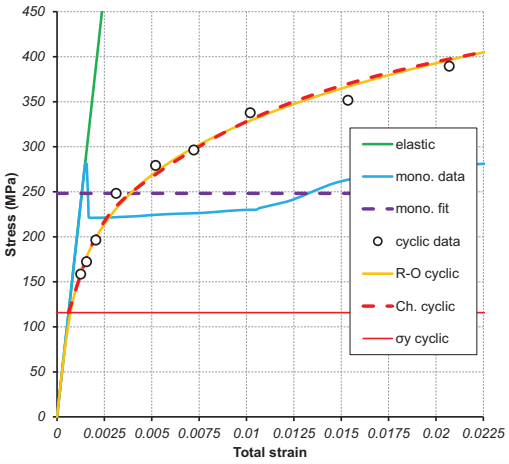

Figure 2: Fitting of monotonic and cyclic SSCs of ASTM A36 steel from [12] at RT

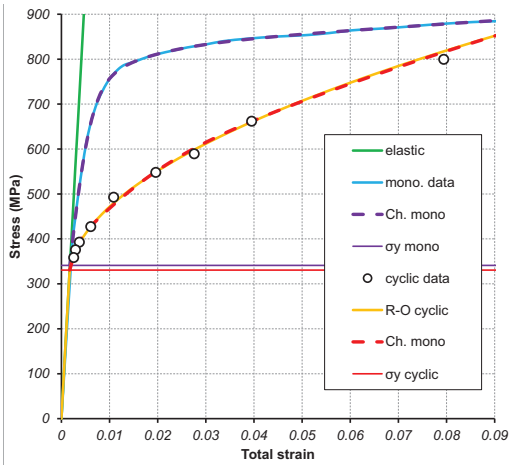

Figure 3: Fitting of monotonic and cyclic SSCs of AISI 4340 steel from [13] at RT

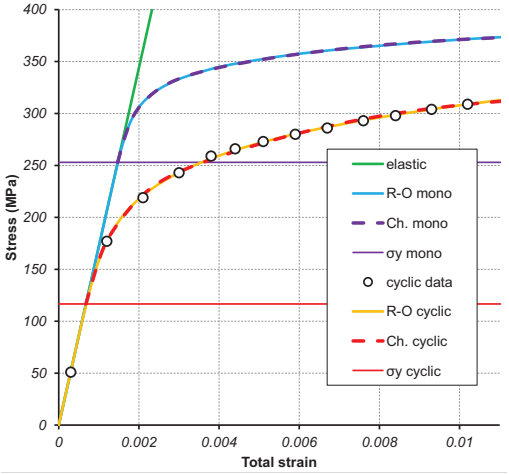

Figure 4: Fitting of monotonic and cyclic SSCs of ASTM P91 steel from [14] at 550°C

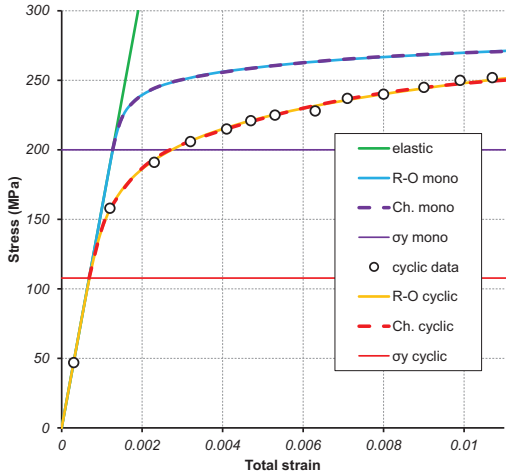

Figure 5: Fitting of monotonic and cyclic SSCs of ASTM P91 steel from [14] at 600°C

non-linear relationship between stress and strain in materials near their yield point. It is particularly useful for metals that harden or soften with plastic deformation showing a smooth elastic-plastic transition. The equations for the monotonic and cyclic SSCs are:

$$\varepsilon^{\text{tot}} = \frac{\sigma}{E} + \left(\frac{\sigma}{B}\right)^{1/\beta} \quad \text{and} \quad \frac{\Delta\varepsilon^{\text{tot}}}{2} = \frac{\Delta\sigma}{2\,E} + \left(\frac{\Delta\sigma}{2\,B}\right)^{1/\beta}, \tag{1}$$

where $\Delta\varepsilon_{\text{tot}}$ is the total strain range and $\Delta\sigma$ is the total stress range (MPa) for each cyclic test respectively; B and β are the R-O material parameters; and Young's modulus E in MPa. Using the value of E, the total strain ε^{tot} in the experimental curves is decomposed into elastic and plastic strain. Then the plastic component ε^{p} of strain is fitted using the the least squares method by the following power-law relations, which are derived from the Eq. (1):

$$\sigma = B\,(\varepsilon^{\text{p}})^{\beta} \quad \text{and} \quad \frac{\Delta\sigma}{2} = B\left(\frac{\Delta\varepsilon^{\text{p}}}{2}\right)^{\beta}. \tag{2}$$

Table 1: Fitting parameters of the Ramberg-Osgood model (1) for different steels and temperatures

Type of plastic material response	Elasto-plastic constants			
	E (MPa)	B (MPa)	β	σ_y (MPa)
ASTM A36 RT cycl.	189606	1015.61	0.2362	–
AISI 4340 RT cycl.*	193053	1897.94	0.5175	320
ASTM P91 RT mono.	215000	710	0.047	–
ASTM P91 RT cycl.		1180	0.155	–
ASTM P91 500°C m.	180000	594	0.066	–
ASTM P91 500°C c.		763	0.15	–
ASTM P91 550°C m.	172000	482	0.054	–
ASTM P91 550°C c.		613	0.144	–
ASTM P91 600°C m.	158000	330	0.042	–
ASTM P91 600°C c.		446	0.123	–
ASTM P91 650°C m.	140000	269	0.071	–
ASTM P91 650°C c.		343	0.125	–

* Extended version of the R-O model (6) is used for data fitting.

The resultant R-O fits for monotonic and cyclic curves are then used to identify the parameters for the Chaboche material model. The range of applicability for the R-O fit is usually quite narrow not exceeding 1% of ε^{tot} depending on the grade of curvature grade for a SSC.

The basic variant of the rate-independent Chaboche model [10, 11] is presented as a combination of nonlinear kinematic hardening and nonlinear isotropic hardening models. The model allows the superposition of several independent backstress tensors and can be combined with any of the available isotropic hardening models. Since in this study monotonic and cyclic SSCs are fitted separately only for the identification of σ_y, only the kinematic hardening component is considered:

$$X = \sum_{i=1}^{N} X_i, \quad \text{with} \quad \dot{X}_i = C_i\,\dot{\varepsilon}^{\text{p}} - \gamma_i\,X_i\,\dot{p}, \tag{3}$$

where $\dot{\varepsilon}^{\text{p}}$ is the plastic strain rate, and $\dot{p}$ is its magnitude. The total backstress X in Eq. (3) is given by the superposition of a number N of kinematic backstresses X_i with a corresponding evolution equation initially proposed by Armstrong & Frederick [16] for $\dot{X}_i$, where C_i and γ_i are kinematic material constants. Chaboche *et al.* [10] recommended $N = 3$ in order to provide a good fit of experimental SSCs, which include large strain areas. Therefore, three backstresses are considered in this study providing an excellent match of the R-O fit (1) for a whole range of strains.

The kinematic hardening constants (C_i, γ_i) and σ_y, which define the size of the yield surface, are identified as recommended in [11]. The cyclic SSC is fitted by the following relation:

$$\frac{\Delta\sigma}{2} = \sigma_y^{\text{c}} + \sum_{i=1}^{N} \frac{C_i}{\gamma_i} \tanh\left(\gamma_i \frac{\Delta\varepsilon^{\text{p}}}{2}\right), \tag{4}$$

which is obtained in [11] by integrating Eq. (3) and considering $\varepsilon^{\text{p}} \approx$ const at the peak stresses for strain-controlled cyclic loading. Relation (4) is valid for the cyclic curve after stabilisation of the hardening or softening effects. Constants (C_i, γ_i and cyclic σ_y^{c}) are identified by automatic fitting Eq. (4) to the R-O extrapolation (2) with "cyclic" values of constants B and β. The identification procedure is implemented in Microsoft Excel using an add-in Solver [17]. The Solver searches for an optimal (minimum in this case) value for a formula in one cell – called the objective cell – subject to constraints, or limits, on the values of other formula cells on a worksheet. The Solver works with a group of cells, called decision variables or simply variable cells, that participate in computing the formulas in the objective and constraint cells. In this case, the Solver adjusts the values in

Table 2: Fitting parameters of the Chaboche model (3)-(5) for different steels and temperatures

Type of plastic material response	Three kinematic hardening backstresses						Yield σ
	C_1 (MPa)	γ_1	C_2 (MPa)	γ_2	C_3 (MPa)	γ_3	$\sigma_{\rm y}$ (MPa)
ASTM A36 RT cycl.	87345.7	984.7	14013.4	111.78	3918.32	13.477	115.792
AISI 4340 RT mono.	205524.6	535.8	8966.94	92.268	782.893	1.0739	341.153
AISI 4340 RT cycl.	35912.1	650.7	6972.29	53.297	4221.72	5.7356	330.727
ASTM P91 RT mono.	1120466	23911	125301.9	2539.9	17295.23	227.86	406.098
ASTM P91 RT cycl.	1030320	11608	136282.4	1254.6	29535.03	148.08	197.493
ASTM P91 500°C m.	1059420	23359	122317.7	2469.7	17631.89	219.49	270.687
ASTM P91 500°C c.	659430	11229	87028.5	1248.7	19146.80	149.22	134.541
ASTM P91 550°C m.	1059420	23359	122317.7	2469.7	17631.89	219.49	270.687
ASTM P91 550°C c.	659430	11229	87028.5	1248.7	19146.80	149.22	134.541
ASTM P91 600°C m.	511703	24975	56536.0	2630.3	7588.97	232.90	199.970
ASTM P91 600°C c.	444752	12216	11344.6	160.13	56238.9	1347.6	107.731
ASTM P91 650°C m.	498277	23543	56252.6	2433.8	8263.19	217.10	115.346
ASTM P91 650°C c.	353928	12801	44816.6	1396.6	8916.41	162.14	80.6307

the decision variable cells containing material constants (C_i, γ_i and $\sigma_{\rm y}^{\rm c}$) in order to minimise the value in the objective cell. This cell contains an average value of the absolute difference between columns containing $\frac{\Delta\sigma}{2}$ calculated by Eq. (2) and Eq. (4) correspondingly in a particular range of $\Delta\varepsilon^{\rm p}$. Applying this approach, an excellent match of Eqs (2) and (4) is achieved.

The monotonic SSC is fitted by the different relation in the following form [11]:

$$\sigma = \sigma_{\rm y}^{\rm m} + \sum_{i=1}^{N} \frac{C_i}{\gamma_i} \left[1 - \exp(-\gamma_i\, \varepsilon^{\rm p})\right], \tag{5}$$

which contains the monotonic $\sigma_{\rm y}^{\rm m}$ and different values of kinematic hardening constants (C_i, γ_i). These constants are identified by fitting Eq. (5) to the R-O extrapolation (2) with "monotonic" values of the R-O parameters B and β. The identification procedure is implemented in Microsoft Excel using an add-in Solver [17] in the same way as for cyclic SSC. An advanced step-by-step guideline for the estimation of the Chaboche viscoplasticity model parameters with their further optimisation was developed by Hyde *et al.* [18].

Application to three structural steels

The above described fitting procedure is applied to SSCs of three structural steels for the purpose of $\sigma_{\rm y}^{\rm m}$ and $\sigma_{\rm y}^{\rm c}$ identification. The first is ASTM A36 steel, with mechanical properties reported in [19, 12], which is a standard low carbon steel, without advanced alloying and is a principal carbon steel employed for bridges, buildings, and many other structural uses. The monotonic SSC for this steel shown in Fig. 2 exhibits perfectly plastic behaviour when reaching the stress of 36 ksi $= 248.211$ MPa in average, which is considered as $\sigma_{\rm y}^{\rm m}$. The perfectly plastic yielding lasts for approximately of $\varepsilon^{\rm p} = 1$ (%) of strain plateau, which is followed by the strain hardening area, then gradually approaching failure at $\varepsilon^{\rm tot} = 30$ (%). The cyclic SSC for this steel shown in Fig. 2 from [12] is fitted by the 2-step procedure, and the obtained material parameters for the R-O (1) and Chaboche (3)-(5) models are listed in Tables 1 and 2 correspondingly.

The second material is AISI 4340 steel [13], a high-strength alloy steel, which has good machinability features and used for a wide range of applications including aircraft landing gears, shafts or axels for power transmission, gears, high pressure pump housings, etc. Both monotonic and cyclic SSCs shown in Fig. 3 and mechanical properties are taken from [13]. Since it is available explicitly, the monotonic SSC is fitted by the Chaboche model (5) directly, and the material parameters are listed in Table 2. The cyclic SSC for this steel shown in Fig. 3 from [13] is available at ten times

wider strain range than for the ASTM A36 steel. Therefore, the R-O model (1) is not able to provide an accurate fit of the cyclic SSC. In this case, the following modification of the R-O equation (1) is used for fitting analysis:

$$\varepsilon^{\text{tot}} = \frac{\sigma}{E} + \left(\frac{\sigma - \sigma_{\text{y}}}{B}\right)^{1/\beta} \quad \text{and} \quad \frac{\Delta\varepsilon^{\text{tot}}}{2} = \frac{\Delta\sigma}{2\,E} + \left(\frac{\Delta\sigma - \sigma_{\text{y}}}{2\,B}\right)^{1/\beta}, \tag{6}$$

Compared to Eq. (1), this notation contains an additional parameter of the yield strength σ_{y} in the meaning of $\sigma_{\text{y}}^{\text{el}}$, and can be applied for an accurate fitting of much wider strain range than Eq. (1). Thus, the cyclic SSC is fitted by the 2-step procedure. The obtained material parameters for the modified R-O (6) and Chaboche (3)-(5) models are listed in Tables 1 and 2 correspondingly.

The third material is ASTM P91 (modified 9Cr-1Mo) steel [20, 14], an advanced ferritic steel with martensitic microstructure, which has already been widely used over the last 2 decades as tubes/pipes for heat exchangers, plates for pressure vessels, and other forged, rolled and cast components for high temperature services. Both monotonic and cyclic SSCs shown in Figs 4 and 5 and mechanical properties at room temperature (RT), 500°C, 550°C, 600°C and 650°C are taken from [14]. Firstly, the monotonic SSCs are presented in [14] by the material parameters for the R-O model (1) listed in Table 1. The cyclic SSCs are presented in [14] by raw data, which is fitted by the R-O model (1) with material parameters listed in Table 1. Secondly, both monotonic and cyclic R-O extrapolations are fitted by the Chaboche model (3)-(5) with material parameters listed in Table 2.

RELATION IN MECHANICAL CHARACTERISTICS

The next step is a check for possible correlations between the obtained yield strength values ($\sigma_{\text{y}}^{\text{m}}$ and $\sigma_{\text{y}}^{\text{c}}$) for ASTM A36, AISI 4340 and ASTM P91 steels and their fatigue and creep behaviour. This identifies a clear similarity for characteristic transition stresses in S-N fatigue, minimum creep strain rate and creep rupture curves, as explained below.

Fatigue behaviour at normal temperature

Engineering structures operating under cyclic loading conditions at normal temperature are usually designed against fatigue failure using the conventional stress-life approach. This approach involves experimental fatigue S-N curves with number of cycles to failure N^* vs. stress. A typical S-N curve is a straight line in double logarithmic coordinates with a distinctive minimum stress lower bound, which is called a fatigue endurance limit (FEL, $\sigma_{\text{lim}}^{\text{f}}$). Referring to [9, 18], $\sigma_{\text{lim}}^{\text{f}}$ is observed for a number of structural steels in benign environmental conditions and represents a stress level below which the material does not fail and can be cycled infinitely without fatigue damage. Comparison of $\sigma_{\text{y}}^{\text{c}}$ defined as material constant and experimentally observed $\sigma_{\text{lim}}^{\text{f}}$ reveals that they are close. This assumption is confirmed by high-cycle fatigue (HCF) experimental data for ASTM A36 [21] and AISI 4340 [22, 23, 24] steels shown in Fig. 6. Comparison of $\sigma_{\text{lim}}^{\text{f}}$ with $\sigma_{\text{y}}^{\text{c}}$ summarised in Table 3 for ASTM A36 steel gives 27.6% accuracy and 5.5% accuracy for AISI 4340 steel. These observations indicate that safe fatigue design is guaranteed in the purely elastic domain defined by $\sigma_{\text{y}}^{\text{c}}$.

Creep behaviour at elevated temperature

Engineering structures operating under constant loading conditions at high temperature are usually designed against creep failure using the conventional time-to-failure approach. This approach involves experimental creep rupture curves with stress vs. time to failure t^*. A typical creep rupture curve is a trilinear smoothed curve in double logarithmic coordinates, with two inflections corresponding to $\sigma_{\text{y}}^{\text{c}}$ and $\sigma_{\text{y}}^{\text{m}}$. These inflections separate three sections on the creep rupture curve, which are characterised by three different creep damage accumulation modes – brittle, ductile and mixed. Three sections with different creep deformations mechanisms can be typically observed

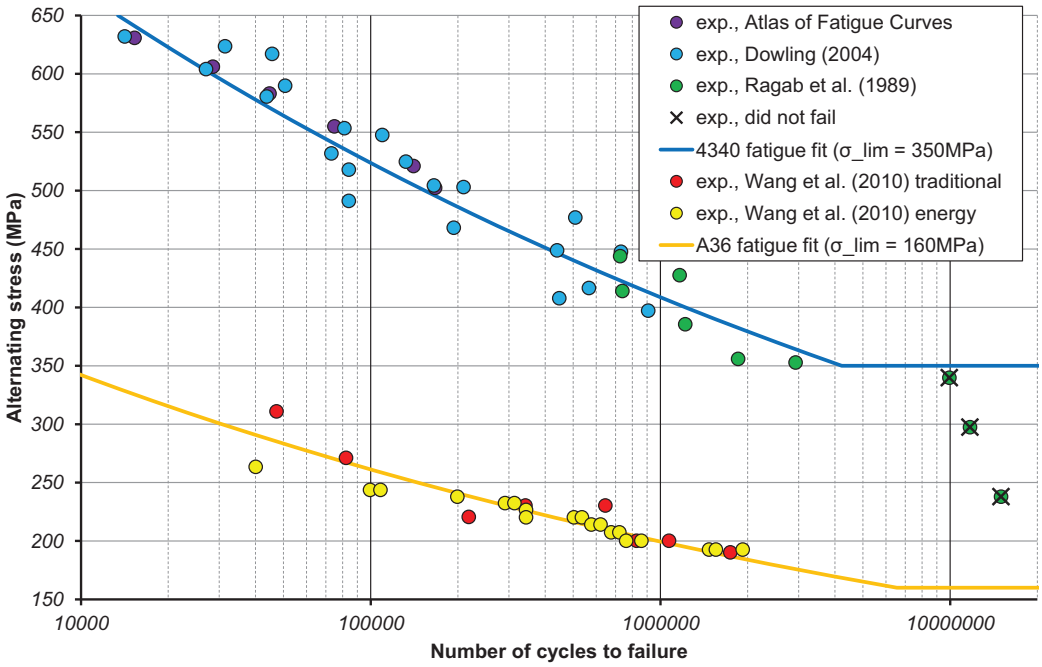

Figure 6: S-N curve fits of ASTM A36 steel based on HCF data by Wang et al. *[21] and AISI 4340 steel based on HCF data from Atlas of Fatigue Curves [22], Dowling [23] and Ragab* et al. *[24]*

on the minimum creep rate curve, presenting minimum creep strain rate vs. stress, which is also a trilinear smoothed curve in double logarithmic coordinates. The deformations mechanism (linear creep, power-law creep and power-law breakdown) are separated by the same two inflections.

This assumption is confirmed by experimental observations for ASTM P91 steel at elevated temperatures. Data for creep rupture shown in Fig. 7 is all taken from the recent study by Kimura [6]. The inflections of corresponding curves were well observed at 600 and 650°C and explained in terms of half monotonic yield ($\sigma_y^{0.2\%}/2$). In contrast to [6], in current study, σ_y^m and σ_y^c from Table 2 are used in combination with test data [6] to provide a basic polylinear fitting. Data for min. creep strain rate shown in Fig. 8 is taken from studies by Sklenička *et al.* [25], Kloc & Fiala [26] and Kimura [20]. The inflections of corresponding curves were observed at 550, 600 and 650°C and explained in terms of transition between different creep deformation mechanisms. As in the case of creep rupture, here the same σ_y^m and σ_y^c from Table 2 are used in combination with test data [20, 26, 25] to provide a basic polylinear fitting. Since the inflections are captured reasonably well on both types of data in Figs 7 and 8, the correspondence of transition stresses on creep rupture and min. creep rate curves proposed by Gorash *et al.* [7, 8] is proved by relating them to σ_y^m and σ_y^c. It should be noted that Dimmler *et al.* [27] associated these inflections with microstructurally determined threshold stresses (back-stress concept). The applicability of this concept was shown using the experimental minimum creep rate and creep rupture curves for several 9-12%Cr heat resistant steels (P91, GX12, NF616, X20 and B2). Dimmler *et al.* [27] emphasised that the knowledge of these threshold stresses limits the range of experimentally based predictions, thus preventing from overestimation of long-term creep rate and creep strength from extrapolated short-term creep data. Therefore, these observations arise a consideration that the most safe creep design is guaranteed in linear creep domain with brittle failure mode, which is also defined by the σ_y^c.

Finally, the fatigue performance of ASTM P91 steel is analysed using the HCF experimental data by Matsumori *et al.* [28] at three different temperatures (RT, 400 and 550°C) illustrated in Fig. 9.

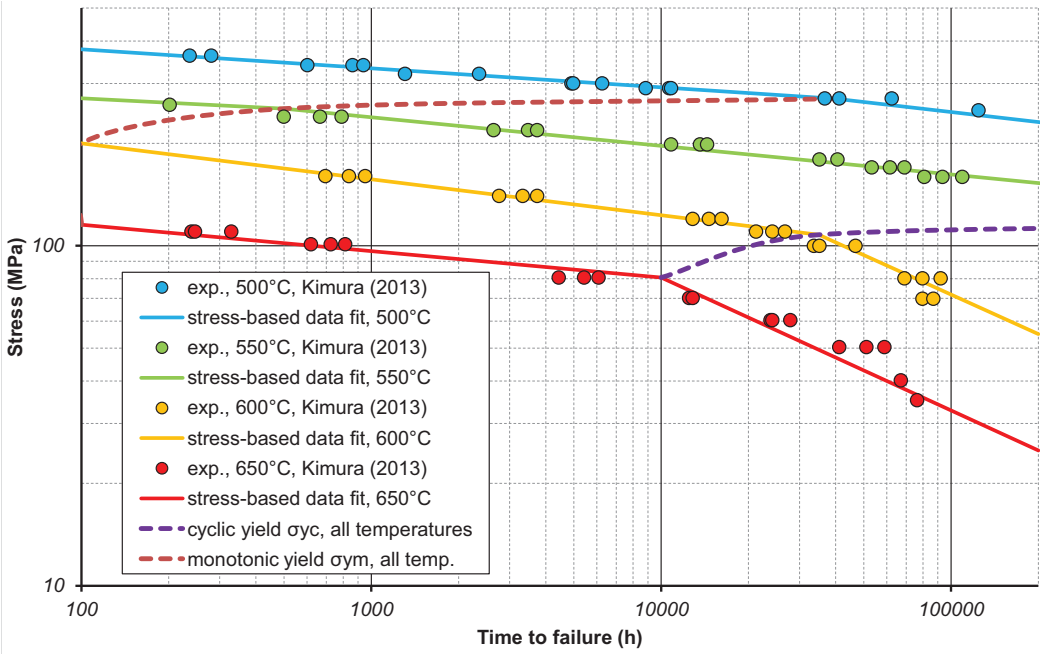

Figure 7: Stress vs. creep rupture life of ASTM P91 steel based on the data by Kimura [6]

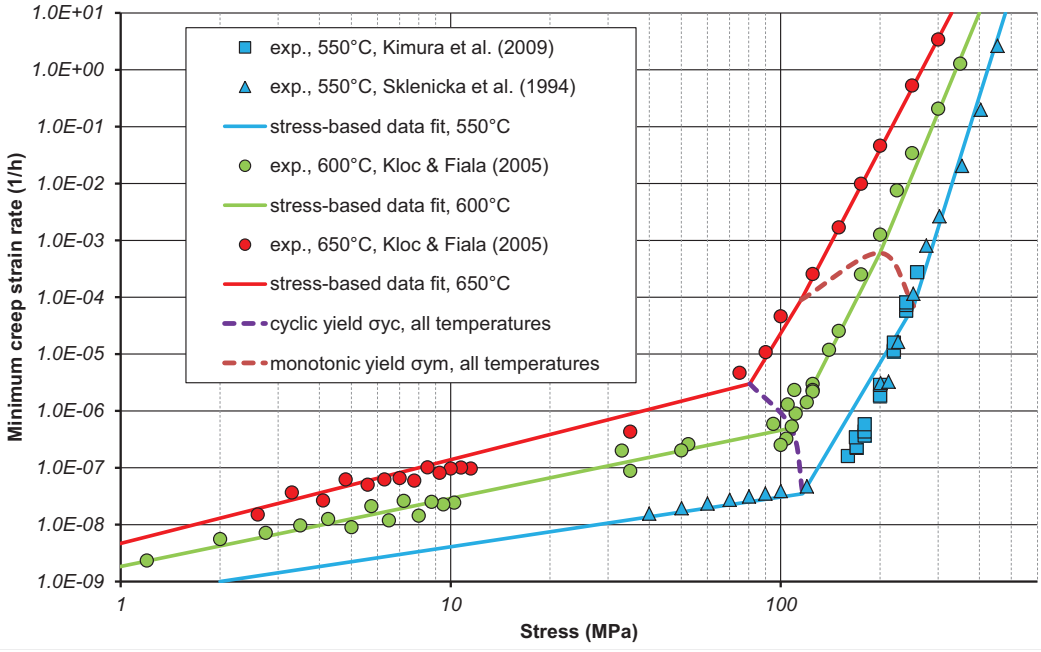

Figure 8: Min. creep rate vs. stress of ASTM P91 steel based on several sets of data [20, 26, 25]

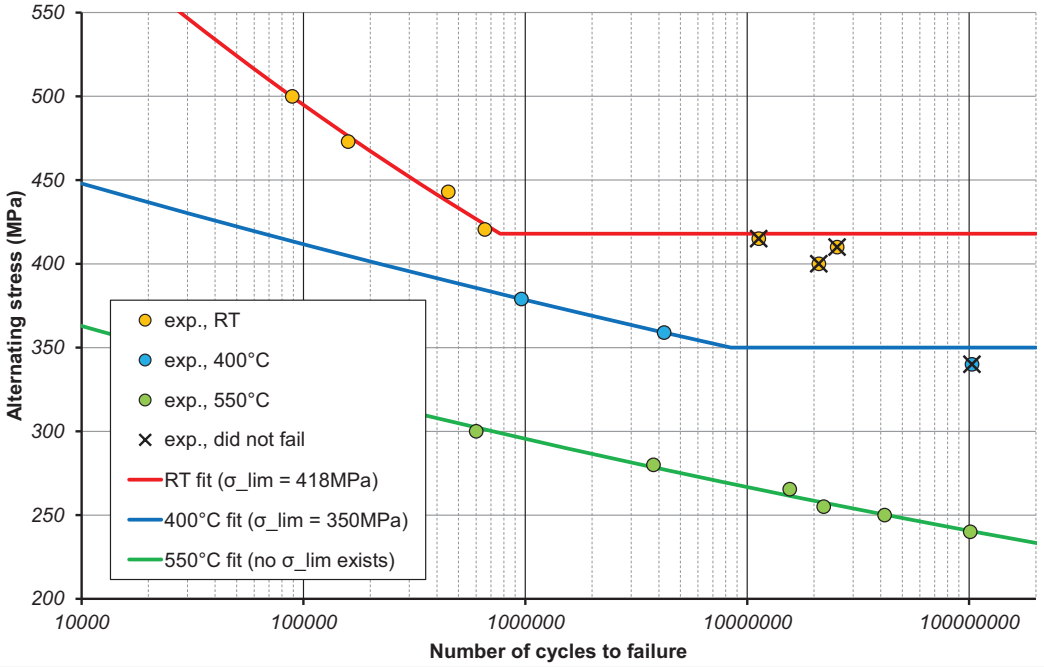

Figure 9: S-N curve fits of ASTM P91 steel based on HCF data by Matsumori et al. *[28]*

From these data, it can be concluded that at elevated temperatures heat-resistant steels don't exhibit $\sigma^{\mathrm{f}}_{\mathrm{lim}}$ on S-N fatigue curves, which is usually observed at normal temperature. The reason for this is the elimination of purely elastic behaviour at high temperature, since there is always some amount of inelastic strain, which is caused by creep. Therefore, there is always a permanent accumulation of creep damage, even at low stress levels and high-strain rate, which leads to inevitable failure. This fact is confirmed by experimental observations [28], which demonstrated the extinction of $\sigma^{\mathrm{f}}_{\mathrm{lim}}$ at 550°C for over 10^8 loading cycles. However, a good match of $\sigma^{\mathrm{f}}_{\mathrm{lim}}$ with $\sigma^{\mathrm{m}}_{\mathrm{y}}$ with accuracy of 2.8% is observed at RT for this steel as shown in Table 3, which makes advanced martensitic steels different from simple ferritic steels is $\sigma^{\mathrm{f}}_{\mathrm{lim}}$ prediction. This effect can be explained by the assumption of Terent'ev [29], who recognised two types of the fatigue endurance limit $\sigma^{\mathrm{f}}_{\mathrm{lim}}$ – standard in HCF range ($N = 10^2$-10^7 cycles) and ultrahigh in gigacycle fatigue (GCF) range ($N = 10^7$-10^{11} cycles). The existence of ultrahigh $\sigma^{\mathrm{f}}_{\mathrm{lim}}$ was proved by the experimental data for high-strength steels (50CrV4, 54SiCrV6 and 54SiCr6), which demonstrated two inflections of the fatigue curves followed by horizontal plateaus – first in HCF area ($N \approx 10^5$-10^6), second in GCF area ($N \approx 10^8$-10^9). The correspondence of $\sigma^{\mathrm{c}}_{\mathrm{y}}$ with ultrahigh $\sigma^{\mathrm{f}}_{\mathrm{lim}}$ for ASTM P91 steel is expected to be found at $N > 10^8$ cycles, but no experimental data is available for this range.

CONCLUSIONS

Kimura's [6] assumption of half monotonic yield ($\sigma^{0.2\%}_{\mathrm{y}}/2$) agrees very well with the outcomes of the current study. According to Table 3, the relation $\sigma^{\mathrm{c}}_{\mathrm{y}} \approx \sigma^{\mathrm{m}}_{\mathrm{y}}/2$ is valid for all temperatures except the highest 650°C. This assumption is not relevant to AISI 4340 steel, which exhibits $\sigma^{\mathrm{c}}_{\mathrm{y}} \approx \sigma^{\mathrm{m}}_{\mathrm{y}}$.

The principal advantage of the $\sigma^{\mathrm{c}}_{\mathrm{y}}$ application to the characterisation of fatigue and creep long-term strength is the relatively fast experimental identification. The total duration of all cyclic tests, which are required to reach the stabilised stress response for the construction of cyclic SSC is much less than the typical durations of fatigue and creep rupture tests at stress levels around $\sigma^{\mathrm{c}}_{\mathrm{y}}$.

Table 3: Comparison of σ_y^m, σ_y^c and σ_{lim}^f for ASTM A36, AISI 4340 and ASTM P91 steels

Steel	ASTM A36	AISI 4340	ASTM P91					
Temp., °C	RT	RT	RT	400	500	550	600	650
σ_y^m, MPa	248.2	341.2	406.1	–	270.7	253.0	200.0	115.3
σ_y^c, MPa	115.8	330.7	197.5	–	134.5	116.6	107.7	80.6
σ_y^m/σ_y^c	2.1	1.0	2.1	–	2.0	2.2	1.9	1.4
σ_{lim}^f, MPa	160.0	350.0	418.0	350.0	–	–	–	–
$\Delta\sigma$, %	27.6	5.5	2.8	–	–	–	–	–

The critical point in the work presented here is an application of the advanced material model (i.e. Chaboche model [10, 11]) to the estimation of a single value of elastic limit σ_y^{el}, which may seem to be complected. However, this approach is effective in typical cases when experimental SSCs are unavailable in explicit form, but available in the form of R-O [15] fittings (1). In other cases, when all necessary experimental SSCs are available in form of raw data, the modified form (6) of the R-O model may reduce the fitting procedure just to one step. Since Eq. (6) contains σ_y as a material parameter, the application of Chaboche model equations (3)-(5) is no longer needed.

REFERENCES

[1] Kim, K. S. *et al.* "Estimation methods for fatigue properties of steels under axial and torsional loading." *Int. J. Fatigue*, vol. 24, no. 7, (2002), pp. 783–793.

[2] Roessle, M. L. and Fatemi, A. "Strain-controlled fatigue properties of steels and some simple approximations." *Int. J. Fatigue*, vol. 22, no. 6, (2000), pp. 495–511.

[3] Casagrande, A. *et al.* "Relationship between fatigue limit and Vickers hardness in steels." *Mater. Sci. & Eng. A*, vol. 528, no. 9, (2011), pp. 3468–3473.

[4] Bandara, C. S. *et al.* "Fatigue Strength Prediction Formulae for Steels and Alloys in the Gigacycle Regime." *Int. J. Mater., Mech. & Manufacturing*, vol. 1, no. 3, (2013), pp. 256–260.

[5] Li, J. *et al.* "Theoretical estimation to the cyclic yield strength and fatigue limit for alloy steels." *Mechanics Research Communications*, vol. 36, no. 3, (2009), pp. 316–321.

[6] Kimura, K. "Creep rupture strength evaluation with region splitting by half yield." *Proc. ASME 2013 PVP Conf.* PVP2013-97819, ASME, Paris, France (Jul. 14-18, 2013), pp. 1–8.

[7] Gorash, Y. Development of a creep-damage model for non-isothermal long-term strength analysis of high-temperature components operating in a wide stress range. PhD thesis, Martin-Luther-University Halle-Wittenberg, Halle (Saale), Germany (Jul. 21, 2008).

[8] Altenbach, H. *et al.* "Steady-state creep of a pressurized thick cylinder in both the linear and the power law ranges." *Acta Mechanica*, vol. 195, no. 1-4, (2008), pp. 263–274.

[9] Dowling, N. E. Mechanical Behavior of Materials: Engineering Methods for Deformation, Fracture, and Fatigue. Pearson Education Limited, Harlow, UK, 4th ed. (2013).

[10] Chaboche, J.-L. *et al.* "Modelization of the strain memory effect on the cyclic hardening of 316 stainless steel." *Trans. 5th Int. Conf. on Structural Mechanics in Reactor Technology*, no. L11/3 in SMiRT5, IASMiRT, Berlin, Germany (Aug. 1979), pp. 1–10.

[11] Chaboche, J.-L. "A review of some plasticity and viscoplasticity constitutive theories." *Int. J. Plasticity*, vol. 24, no. 10, (2008), pp. 1642–1693.

[12] Higashida, Y. and Lawrence, F. V. Strain controlled fatigue behavior of weld metal and heat-affected base metal in A36 and A514 steel welds. *FCP Report No. 22*, University of Illinois, Urbana, Illinois, USA (Aug. 1976).

[13] Smith, R. W. *et al.* Fatigue behavior of materials under strain cycling in low and intermediate life range. *Technical Note No. D-1574*, NASA, Cleveland, Ohio, USA (Jan. 1963).

[14] Data sheets on elevated-temperature, time-dependent low-cycle fatigue properties of ASTM A387 Grade 91 (9Cr-1Mo) steel plate for pressure vessels. *NRIM Fatigue Data Sheet No. 78*, National Research Institute for Metals, Tokyo, Japan (Dec. 25, 1993).

[15] Ramberg, W. and Osgood, W. R. Description of stress-strain curves by three parameters. *Technical Note No. 902*, NASA, Washington DC, USA (Jul. 1943).

[16] Armstrong, P. J. and Frederick, C. O. A mathematical representation of the multiaxial Bauschinger effect. *Report No. RD/B/N731*, CEGB, Berkeley, UK (Dec. 1966).

[17] Microsoft® Office Professional Plus. Excel Help System // Analyzing data // What-if analysis // Define and solve a problem by using Solver. Microsoft Corp., Release 2010 ed. (2009).

[18] Hyde, T. *et al.* Applied Creep Mechanics. McGraw-Hill Education, New York, USA (2004).

[19] ASTM Standard. Standard Specification for Carbon Structural Steel. A36/A36M – 08, West Conshohocken, USA (2008).

[20] Kimura, K. *et al.* "Long-term creep deformation property of modified 9Cr-1Mo steel." *Mater. Sci. & Eng. A*, vol. 510-511, (2009), pp. 58–63.

[21] Wang, X. G. *et al.* "Quantitative Thermographic Methodology for Fatigue Assessment and Stress Measurement." *Int. J. of Fatigue*, vol. 32, no. 12, (2010), pp. 1970–1976.

[22] Boyer, H. E. Atlas of Fatigue Curves. ASM International, Materials Park, Ohio, USA (1986).

[23] Dowling, N. E. "Mean Stress Effects in Stress-Life and Strain-Life Fatigue." *SAE Technical Paper*, , no. 2004-01-2227, (2004), pp. 1–14.

[24] Ragab, A. *et al.* "Corrosion Fatigue of Steel in Various Aqueous Environments." *Fatigue Fract. Engng Mater. & Struct.*, vol. 12, no. 6, (1989), pp. 469–479.

[25] Sklenička, V. *et al.* "Creep Behaviour and Microstructure of a 9Cr Steel." D. Coutsouradis *et al.*, ed., *Proc. Conf. Materials far Advanced Power Engineering 1994*. Part I, Kluwer Academic Publishers, Liège, Belgium (Nov. 3-6, 1994), pp. 435–444.

[26] Kloc, L. and Fiala, J. "Viscous creep in metals at intermediate temperatures." *Kovové Materiály*, vol. 43, no. 2, (2005), pp. 105–112.

[27] Dimmler, G. *et al.* "Extrapolation of short-term creep rupture data – The potential risk of over-estimation." *Int. J. of Pressure Vessels & Piping*, vol. 85, (2008), pp. 55–62.

[28] Matsumori, Y. *et al.* "High Cycle Fatigue Properties of Modified 9Cr-1Mo Steel at Elevated Temperatures." *Proc. ASME 2012 Int. Mechanical Engineering Congress & Exposition*. IMECE2012-87329, ASME, Houston, Texas, USA (Nov. 9-15, 2012), pp. 85–89.

[29] Terent'ev, V. F. "Endurance limit of metals and alloys." *Metal Sci. & Heat Treatment*, vol. 50, no. 1-2, (2008), pp. 88–96.